J. Membrane Biol. 20, 269–300 (1975)

Charge Pulse Studies of Transport Phenomena in Bilayer Membranes

I. Steady-State Measurements of Actin- and Valinomycin-Mediated Transport in Glycerol Monooleate Bilayers

Stephen W. Feldberg and George Kissel

Brookhaven National Laboratory, Upton, New York 11973

Received 13 June 1974; revised 25 September 1974

Summary. A charge pulse technique has been applied to studies of transport phenomena in bilayer membranes. The membrane capacitance can be rapidly charged (in less than a microsecond). The charge then decays through the membrane's conductive mechanism—no current flows through the solution or external circuitry. The resulting voltage decay is thus a manifestation of membrane and boundary layer phenomena only. There are a number of advantages to this approach over conventional voltage or current-clamp techniques: the rise-time of the voltage perturbation is not limited by the time constant deriving from the membrane capacitance and solution resistance, thus permitting study of extremely rapid rate processes; the membrane is exposed to high voltage for relatively short times and thus can be subjected to higher voltages without breakdown; the steady-state current-voltage behavior of the membrane can be deduced from a single charge pulse experiment; the charge (and therefore the integral of the ion flux through the membrane) is monitored allowing detection of rate processes too rapid to follow directly. In this paper we present what is primarily a steady-state analysis of actin (non-, mon-, din-, trin-)-mediated transport of ammonium ion and valinomycin-mediated transport of cesium and potassium ions through glycerol monooleate bilayers. We introduce the concept of the "intercept discrepancy", a method for measuring charge lost through extremely rapid rate processes. Directly observable pre-steady-state phenomena are also discussed but will be the main subject of part II.

Glossary of Symbols

Symbol	*Units*	*Definition*
$\mathscr{K}_m$	Farads/cm^2	Specific membrane capacitance
$\mathscr{K}_e$	Farads/cm^2	Specific capacitance of electrode
A_m	cm^2	Membrane area
A_e	cm^2	Electrode area
R_s	ohms	Effective resistance of solution between membrane and each electrode

Symbol	*Units*	*Definition*
R_e	ohms	Electrode resistance
$G(V, t)$	$\text{ohm}^{-1}\,\text{cm}^{-2}$	Specific conductance of membrane (function of voltage and time)
V	volts	Voltage across membrane
V_e', V_e''	volts	Potential of left and right electrode *vs.* solution
u	dimensionless	$FV/(RT)$
F	coul/mole	Faraday $= 9.65 \times 10^4$ coul/mole
RT	volt coul/mole	Gas constant $\times$ temp (at 26 °C) $= 2.49 \times 10^3$ volt coul/mole
V_i	volts	Intercept voltage
V_1, V_2, V_3	volts	Specific intercept voltages—*see* Theory section
q^0	coul/cm^2	Magnitude of charge pulse per unit area of membrane
Γ_s, Γ_{is}	mole/cm^2	Surface concentration of free carrier and ion-carrier complex at equilibrium
Γ_T	mole/cm^2	$\Gamma_T = \Gamma_s + \Gamma_{is}$
c_i	mole/cm^3	Concentration of permeant ion in aqueous phase
c_s	mole/cm^3	Concentration of carrier in bulk lipid/hydrocarbon mixture
k_1	$\text{cm}^3\,\text{mole}^{-1}\,\text{sec}^{-1}$	Heterogeneous rate constant for formation of Γ_{is} [*see* Eq. (7)]
k_{-1}	sec^{-1}	Heterogeneous rate constant for dissociation of Γ_{is} [*see* Eq. (7)]
K_1	cm^3/mole	Equilibrium constant [*see* Eq. (8)]
β	mole/cm^2	*See* Eqs. (5) and (6)
k_s	sec^{-1}	Rate constant for transport of free carrier across the membrane
k_{is}', k_{is}''	sec^{-1}	Voltage-dependent rate constants for transport of ion carrier complex across membrane from left to right and from right to left, respectively
k_{is}^*	sec^{-1}	Standard rate constant (voltage independent) for transport of ion complex halfway across the membrane [*see* Eqs. (9) and (10) and footnote 4]
ϕ, ϕ_m	dimensionless	Height of Eyring barrier at peaks and at midpoint (*see* Fig. 2)
n	dimensionless	Position parameter for peaks of Eyring barrier (*see* Fig. 2)
J_{is} $J_{is}(V, t=\infty)$	moles $\text{sec}^{-1}\,\text{cm}^{-2}$	Steady-state flux of ions across the membrane
$J_{is}(V, t)$	moles $\text{sec}^{-1}\,\text{cm}^{-2}$	Flux of ions across the membrane as a function of voltage and time
a	$(\text{cm}^3/\text{mole})^{\frac{1}{2}}\,\text{sec}^{-1}$	*See* Eqs. (14) and (15)
ω	dimensionless	Relative chemical capacitance [*see* Eq. (17)]

The purpose of this paper is to demonstrate the applicability of a charge pulse technique for measuring the electrical manifestations of ion transport across bilayer lipid membranes. The technique is ideally suited to measuring both steady-state and relaxation phenomena.

In this paper we evaluate steady-state behavior of antibiotic-mediated alkali ion transport. In addition, we will demonstrate how to measure quantitatively the amount of free carrier and carrier-ion complex within the membrane, and thereby, in certain cases, evaluate the kinetic parameters.

A bilayer lipid membrane (BLM) separating a pair of electrodes in two conducting media can present a variety of problems to an investigator attempting to ascertain its electrical properties. Most obvious, of course, are problems relating to the stability and reversibility of the measuring electrodes. These are easily overcome by careful electrode selection and construction. With highly conducting membranes a problem arises when the solution and membrane conductances are of comparable magnitude, and in relaxation studies there is the added difficulty of rapidly charging the membrane capacitance to the desired potential through the solution resistance and through any other resistance that may be present in the system [e.g. a resistor for measuring the current flowing during a voltage clamp experiment (Benz, Stark, Janko & Läuger, 1973)].

A charge pulse technique has been used previously in membrane studies (e.g. Hodgkin, Huxley & Katz, 1952) but we follow more closely the electrochemical approach described by several authors whose primary interest was electrode kinetics and adsorption at electrode-solution interfaces (Delahay, 1962; Reinmuth, 1962; Weir & Enke, 1967; Daum & Enke, 1969; Kudirka, Daum & Enke, 1972; Kudirka & Enke, 1972). The principles of application of the method to membrane studies are straightforward. The membrane (Fig. 1) may be considered as a capacitive element $\mathscr{K}_m$ in parallel with a conductive element ($G(V, t)$). The ideal charge pulse contains a precisely known charge which is injected in an infinitely small time.[1] At all times other than the instant of charge injection the pulse generator must present an effectively infinite impedance to the system.[2] A voltage is instantaneously developed across capacitive element which then decays through the conductive element. There is virtually no current in the external circuit and thus error due to voltage drop $2i\,R_s$ is eliminated. The details of

1 A commercial pulsing device (e.g. Chronetics, Inc.) has a 20 nsec rise-time to maximum current of 400 mamps.

2 A commercial pulser may need to be modified to increase its open circuit impedance by inserting a back-biased diode in the output circuit (C. G. Enke, *personal communication*).

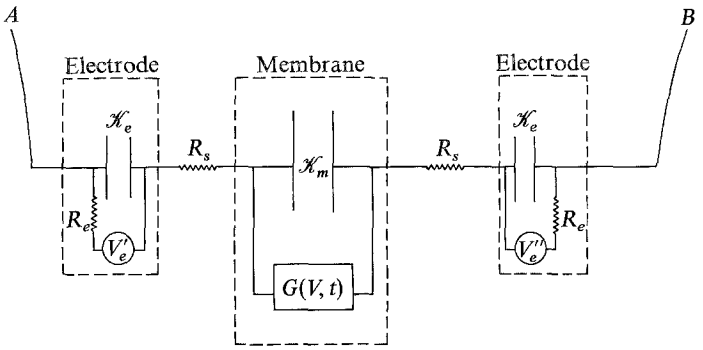

Fig. 1. Electrical analog for BLM separating two electrically similar solution-electrode pairs. Charge injection and voltage monitoring occur at points *A* and *B*. *See* Glossary of Symbols for definitions

this voltage decay are a manifestation of the rate processes associated with the membrane conductance. If these processes are rapid relative to the time constant of decay, they may be assumed to be at steady state and

$$\frac{G(V)}{\mathscr{K}_m} = d \ln V / dt. \tag{1}$$

The assumption that the membrane capacitance is voltage independent shall be proved valid, and this of course simplified interpretation of the data. For this reason we believe that the charge pulse technique is more ideally suited to studies of membrane phenomena than to electrode phenomena where the double-layer capacitance can vary significantly with small changes in potential (*see*, for example, review by Mohilner, 1966).

The advantages that accrue to this method are the following:

(1) The entire conductance-voltage relationship can be deduced from data obtained by a single pulse on a single membrane and in a time short enough to minimize changes in membrane area and composition.

(2) Because the voltage across the membrane decays rapidly it is possible to determine membrane capacitance and conductance at high voltages that would, if sustained, break the membrane.

(3) Because the perturbation is predetermined it is possible to inject charge and change the membrane potential without the $2R_s \mathscr{K}_m A_m$ (Fig. 1) limiting time constant of a voltage-clamp technique.

(4) The decay of the voltage across the membrane capacitance through the membrane conductance does not pass current through the external

circuit. Thus, the solution resistance between the membrane and the electrodes does not introduce an extraneous voltage drop.

(5) The time course of the voltage decay depends on the ratio $\mathscr{K}_m/G(V, t)$ which is independent of membrane area.

(6) By using large electrodes with a large double-layer capacitance relative to the membrane capacitance (*see* Fig. 1, $\mathscr{K}_e A_e/(\mathscr{K}_m A_m) \gg 1$) the electrodes will present virtually zero impedance during the charging process. In fact, unless accurate measurements of the equilibrium potentials are desired, platinum electrodes will work as well as a reversible silver or calomel electrode.

(7) Because of the short time and the small amount of charge passed, concentration polarization in the unstirred boundary layer adjacent to the membrane is minimized.

(8) Because the membrane capacitance and the quantity of charge injected can be accurately determined, the voltage across the membrane at any time after injection allows one to measure precisely how much charge has been moved through the conductive path. The extrapolation of the voltage *vs.* time curve back to zero time should intercept the voltage axis at a potential corresponding exactly to

$$V_i = q^0/\mathscr{K}_m. \tag{2}$$

Any discrepancy, e.g.

$$q^0/\mathscr{K}_m - V_i > 0 \tag{3}$$

is indicative of a fast, short-lived conduction path whose time constant may be too short to be resolved but whose amplitude is clearly manifested.

The primary disadvantage of the technique is that the relaxation occurs over a broad potential range and the voltage dependencies as well as the time dependencies must be determined. Furthermore, small amplitude relaxations will be difficult to observe and analyze. Unlike the voltage-clamp technique where any deviation of the current time curve from a flat response is the manifestation of a relaxation process, there is always the fundamental $\frac{\mathscr{K}_m}{G(V, t)}$ time constant decay in the charge pulse technique, and deviations are less obvious.

Theory

Steady-State

The equations we present here for the steady-state carrier-mediated transport are based on Hladky's presentation (Hladky, 1972) of Läuger and

Stark's model (Läuger & Stark, 1970; Stark & Benz, 1971). In this paper we concern ourselves only with the symmetrical case where the compositions of the salt solutions on each side of the membrane are identical. We have modified the notation, using the symbol Γ to denote concentrations of species on or near each membrane surface in moles/cm^2. We feel that this notation is more consistent with the evidence that carrier and carrier-ion complex are concentrated in a planar region located just inside the polar head group on each side of the bilayer (Hsu & Chan, 1973), a fact that had long been assumed primarily for the sake of mathematical simplification. We also assume that all carrier molecules (complexed or uncomplexed) are membrane bound in the time scale of the experiments and that a given carrier concentration in the bulk lipid/*n*-decane mixture establishes a given concentration of free carrier in the BLM. We also use concentration c_i rather than activity a_i. The reader will note that concentrations are expressed in moles/cm^3. Thus the constants we report are the formal constants for the particular ionic medium being used. We do maintain constant ionic strength (3.0×10^{-3} moles/cm^3) for all our experiments. The Läuger-Stark-Hladky equation, then, with modified notation is

$$J_{is} = \frac{\beta \dfrac{k_1}{k_{-1}} c_i (k'_{is} - k''_{is})}{\left[1 + \dfrac{k'_{is} + k''_{is}}{k_{-1}} \left(1 + \dfrac{k_1 c_i}{2k_s}\right)\right]} \tag{4}$$

where

$$\beta = \Gamma_s \tag{5}$$

when free carrier in the BLM is buffered, or

$$\beta = \frac{\Gamma_T}{1 + K_i c_i} \tag{6}$$

when total carrier in BLM is maintained constant. The pertinent surface reactions are

$$c_i + \Gamma_s \underset{k_{-1}}{\overset{k_1}{\rightleftarrows}} \Gamma_{is} \tag{7}$$

and

$$K_1 = k_1 / k_{-1}. \tag{8}$$

The prime (′) and double prime (″) denote rate processes moving molecules across the membrane from left to right and right to left, respectively. We tacitly assume that the surface rates, k_1 and k_{-1}, are potential independent

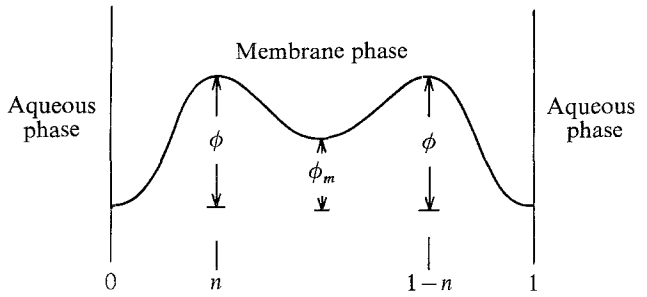

Fig. 2. Symmetrical double Eyring barrier. Numbers 0, n, $1-n$, and 1, are values of x/δ (δ=thickness of membrane) at the left membrane-water interface, the first barrier peak, the second barrier peak, and the right membrane-water interface, respectively

and at present we have no data to counter this. It is clear from Eq. (4), however, that the potential dependence of k_{-1} is intimately coupled to that of k'_{is} and k''_{is}. Only direct relaxation measurements to determine values of k'_{is} and k''_{is} could separate these dependencies (Stark, Ketterer, Benz & Läuger, 1971; Benz *et al.*, 1973).

The voltage dependence for k'_{is} and k''_{is} which best explains our data can be derived assuming a double Eyring barrier (Fig. 2).[3] The resulting expressions for steady state are

$$k'_{is}=\tfrac{1}{2}k^*_{is}\frac{e^{u/2}}{\cosh\left(\left(\tfrac{1}{2}-n\right)u\right)} \tag{9}$$

$$k''_{is}=\tfrac{1}{2}k^*_{is}\frac{e^{-u/2}}{\cosh\left(\left(\tfrac{1}{2}-n\right)u\right)}. \tag{10}$$

The standard rate constant k^*_{is},[4] includes the exponential $e^{-\phi}$. The height of the barrier at the midpoint of the membrane ϕ_m cancels out of the mathematical expressions. We assume a reasonably high value of ϕ_m since a small ϕ_m would favor entrapment of a significant fraction of the carrier complex in the central region. Benz *et al.* (1973) suggest such an entrapment for *free* valinomycin in a neutral phospholipid BLM.

3 Seelig and Niederberger (1974) and McConnell (1974) have shown that the lipid hydrocarbon tails exhibit maximum fluidity in the innermost region of the membrane. This suggests that resistance to translocation might be highest near the polar head groups and is consistent with a double Eyring barrier model or a Nernst-Planck diffusion model with a trapezoidal barrier (Hall, Mead & Szabo, 1973).

4 The constant k^*_{is} is really the standard rate constant for crossing each of the Eyring barriers (Fig. 2). In other words, it is the rate constant for an ion complex to move halfway across the membrane. Thus, it will be double the value of the corresponding rate constant for a jump across a single Eyring barrier.

Combining Eqs. (6), (9) and (10) gives a generalized steady-state flux expression:

$$J_{is}=\frac{\beta\frac{k_1}{k_{-1}}c_i k_{is}^*\frac{\sinh(u/2)}{\cosh\left(\left(\frac{1}{2}-n\right)u\right)}}{\left[1+\frac{k_{is}^*}{k_{-1}}\frac{\cosh(u/2)}{\cosh\left(\left(\frac{1}{2}-n\right)u\right)}\left(1+\frac{k_1 c_i}{2k_s}\right)\right]}. \tag{11}$$

When $n=\frac{1}{2}$, and with cognizance of footnote 4, Eq. (11) becomes identical to the expression derived for a single Eyring barrier model (Läuger & Stark, 1970; Stark & Benz, 1971; Ciani, Eisenman, Laprade & Szabo, 1973). A virtually congruent set of current-voltage curves can be obtained assuming Nernst-Planck diffusion across a membrane with a trapezoidal barrier (Hall *et al.*, 1973) where n corresponds approximately to the position of the corners of the trapezoid.

The expression for the decay of the voltage across the membrane capacitance through the conductive path is

$$\frac{dV}{dt}=J_{is}\frac{F}{\mathscr{K}_m} \tag{12}$$

$$\frac{d\ln V}{dt}=\frac{J_{is}F^2}{RT\mathscr{K}_m u}. \tag{13}$$

Combining Eqs. (11) and (13) and numerically integrating gives the desired voltage-time transient. The *shape* of the curve is determined by the values of n, k_{is}^*/k_{-1}, and $\left(1+\frac{k_1 c_i}{2k_s}\right)$. The *scale* is determined by the parameter $\frac{\beta k_1}{k_{-1}}c_i k_{is}^* F^2 t/(RT\mathscr{K}_m)$. If Eq. (6) obtains, $K_1 c_i$ and thus K_1 can be evaluated under certain conditions as will be demonstrated. To evaluate n we invoke what may well be two dangerous assumptions: (1) for a given carrier the value of n will be independent of the particular alkali ion transported, and (2) the reaction coordinate for reaction (7) does not change greatly as the alkali ion is changed. The shift in the free energy curves of the reactants and products, corresponding to a change in the value of K_1, will change the activation energy of the forward and reverse reactions so that the following is approximately true:[5]

$$k_1\approx a\sqrt{K_1} \tag{14}$$

$$k_{-1}\approx a/\sqrt{K_1}. \tag{15}$$

5 This is a highly simplified variation of Marcus' theory relating rates of a homogeneous electron transfer to the equilibrium constant for the reaction (*see* Marcus, 1963).

Thus, the smaller the value of K_1, the more likely it is that Eq. (11) is operating in the equilibrium domain (i.e. k_{is}^*/k_{-1} is sufficiently small that the second term in the denominator of Eq. (11) will be effectively zero at all potentials).

The values of the remaining parameters are determined for a particular alkali ion by fitting the integrated form of Eq. (11) to the voltage-time curve.

Determination of Γ_{is} and Γ_T: The Intercept Discrepancy Method

Under certain conditions the charge pulse method allows a direct measurement of Γ_{is} and Γ_T. Immediately after charge pulse injection across a membrane in equilibrium, there is a shift in the surface concentrations of the carrier and carrier complex as the system moves from equilibrium to steady state. A quantity of charge is consumed in excess of that predicted solely on the basis of the steady-state current. With adequately fast pulsing and data acquisition systems the resulting voltage decay transient could be directly observed. In any case, the amplitude of this transient can be observed. The extrapolation of the steady-state voltage decay back to zero time gives a voltage intercept that is lower than the zero-time voltage predicted on the basis of membrane capacitance and the quantity of injected charge [Eq. (3)]. This difference between the two voltages (the intercept discrepancy) is directly related to Γ_{is} and Γ_T.

Under conditions of adequately high voltage we can consider the rate process k'_{is} to be effectively infinite, and k''_{is} to be zero. Eq. (11) becomes voltage independent and thus the steady-state voltage decay will be linear. The intercept discrepancy will reflect not only the carrier complex Γ_{is} that will have moved virtually instantaneously from one side of the membrane to the other, but also some Γ_s which converts to Γ_{is} through reaction (7). We have calculated the normalized flux integral $\int_0^t J_{is}(V=\infty, t)\, dt/\Gamma_T$ as a function of normalized time $k_{-1}t$ for the following conditions: $k''_{is}=\infty$, $k'_{is}=0$, and $K_1 c_i=1.0$. The variable parameter is the term $k_1 c_i/k_s$. The graph of these relationships is shown in Fig. 3. The solid lines must all have the same zero-time intercept of 0.5 corresponding to the Γ_{is} instantaneously moved across the membrane ($\Gamma_{is}/\Gamma_T=0.5$ when $K_1 c_i=1.0$). The dashed lines are the extrapolations of the straight line (steady state) portions of the curves to zero time. In principle then, with perfect electronics, and large values of the parameter $k_1 c_i/k_s$, one ought to be able to determine three voltage intercepts, and deduce both Γ_{is} and Γ_T. The first voltage intercept, $V_1=q^0/\mathscr{K}_m$, corresponding to the beginning of the very rapid transport

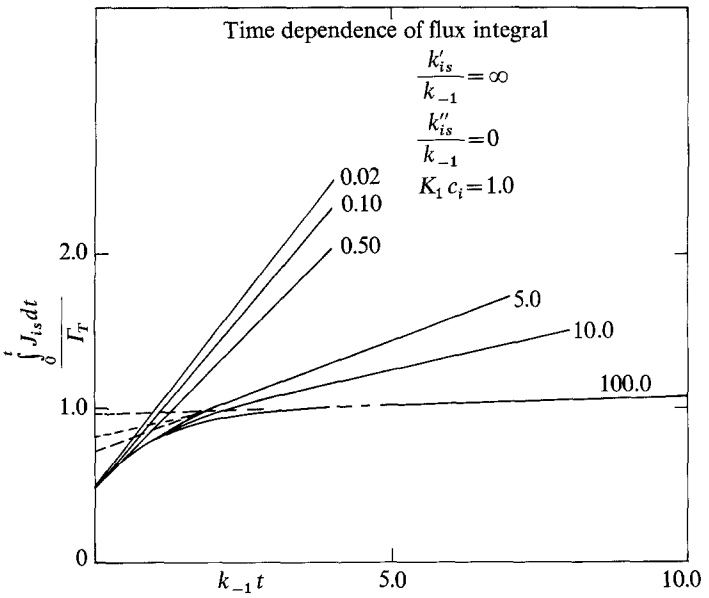

Fig. 3. Time dependence of flux integral. Integral $\int_0^t J_{is}(V=\infty, t)\, dt/\Gamma_T$ as a function of normalized time, $k_{-1}\, t$, for the condition $K_1 c_i=1.0$. Number to the right of each curve is value of parameter $k_1 c_i/k_s$ for that curve. Dashed line is extrapolation of steady-state portion of a given curve to $t=0$

of Γ_{is} across the membrane, may be impossible to see even under the best of circumstances. This will of course depend on the membrane lipid used as well as the speed of the electronic equipment. Nevertheless, V_1 can be calculated from q^0 and $\mathscr{K}_m$. The second intercept, V_2, corresponds to the completion of the Γ_{is} transport (zero-time intercept of solid curves in Fig. 3) and the onset of Γ_s conversion to Γ_{is}. The third intercept, V_3, corresponds to the extrapolation of the steady-state voltage decay back to zero-time.

The voltage discrepancy, $V_1 - V_2$, corresponds directly to Γ_{is}. Thus, it is clear that with improved electronics or membranes with slower rate processes (than those obtaining in glycerol monooleate) that both Γ_{is} and Γ_s can be measured in a single pulse experiment.

In practice, it is most likely that only V_3 can be measured experimentally and V_1 calculated from q^0 and $\mathscr{K}_m$. We can see from Fig. 3 that there are two well-defined limiting cases: (1) when $k_1 c_i/k_s$ is small the intercept corresponds to Γ_{is} alone (0.5 in this case), and (2) when $k_1 c_i/k_s$ is large the intercept corresponds to Γ_T.

The experimental intercept discrepancy depends on these same phenomena and relates to Γ_{is} and Γ_T in the following general way:

$$\Gamma_{is} \leqq \frac{\Delta V \mathscr{K}_m}{F} \leqq \Gamma_T. \tag{16}$$

Implicit in this equation is the assumption that the carrier complex moves across the entire bilayer when in fact it probably moves only across an inner region between the polar head groups. Thus the effective capacitance may be somewhat larger than $\mathscr{K}_m$ and the true values of Γ_{is} and Γ_T proportionately larger.

There is a final practical consideration: the experimental visibility of the intercept discrepancy. With perfect electronics or with adequately slow rate processes, V_1 and V_2 and/or V_3 can be determined in a single charge pulse experiment. Then, we might anticipate that discrepancies of a few millivolts (e.g. 10 mV) could be measured with reasonable precision. If, on the other hand, we are dependent upon a calculated value of V_1, other experimental variables must be considered (e.g. A_m or q^0) and a larger intercept discrepancy is required for reasonable precision (e.g. 50 mV). The magnitude of the intercept discrepancy will depend approximately on the following ratio

$$\omega = \frac{\Gamma_{is} F^2}{\mathscr{K}_m RT} = \Delta V \cdot \frac{F}{RT} \tag{17}$$

relating the chemical and electrical capacitance of the membrane. For a minimum 50 mV response, $\omega \geqq 2$. Interestingly, a value of ω that is too large leads to experimental difficulties. Enough charge is dissipated during the initial transient so that the voltage drops too low to maintain $k'_{is} = \infty$.

Materials and Methods

The bulk membrane material used throughout this study comprised 5% (by volume) glycerol monooleate (GMO) in *n*-decane (both materials were obtained from Matheson, Coleman and Bell and used without further purification). In one experiment 5% ethyl acetate (reagent-grade) was added. Valinomycin was purchased from Calbiochem. Nonactin was a gift from the Squibb Institute for Medical Research, Princeton, New Jersey. The CIBA Pharmaceutical Company provided us with nonactin, monactin, dinactin and trinactin. The antibiotics were used as received.

Salt solutions were prepared from reagent-grade chemicals (used without further purification) and doubly distilled water. Solutions were filtered through a Whatman 42 filter to remove dust and particulates.

The antibiotics were dissolved directly in the bulk membrane material on a weight/volume basis, following the suggestion of Stark and Benz (1971). The aqueous phases

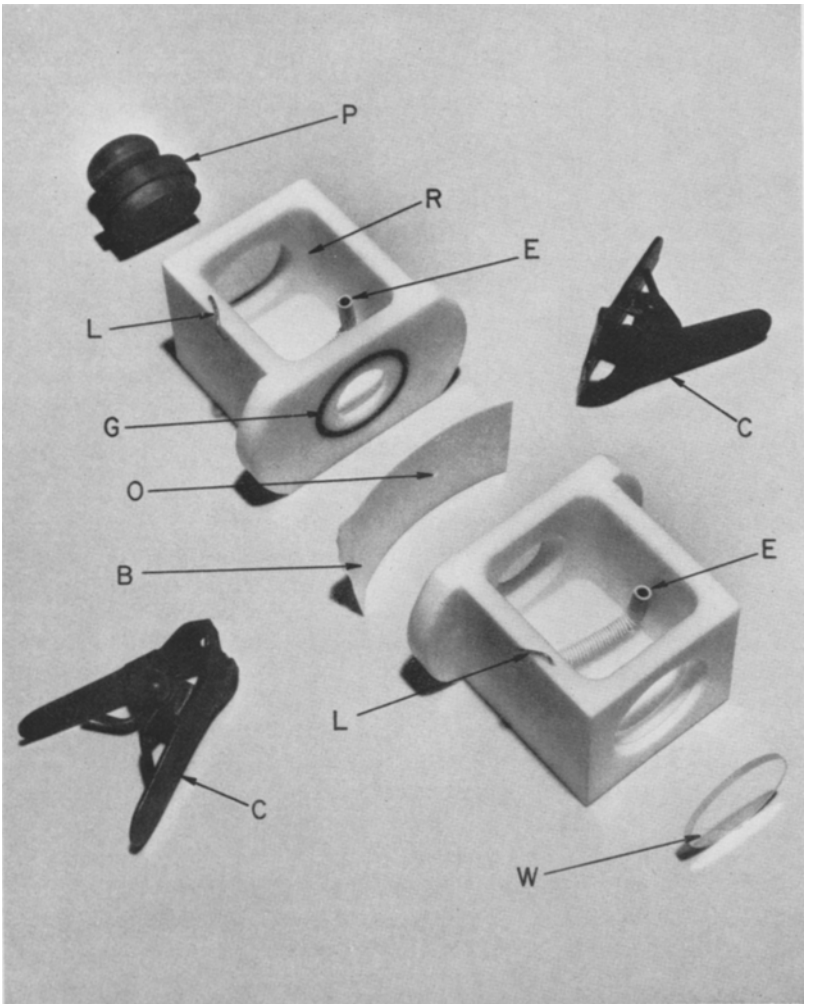

Fig. 4. Three piece cell. Components: *B*, 10-mil teflon barrier; *C*, clamps; *E*, silver coil electrodes; *G*, inset O-ring; *L*, electrode leads; *O*, orifice for BLM formation; *P*, black plug; *W*, optical window. Overall length approximately 9 cm

were *not* stirred during these experiments in order to minimize extraction of carrier from the BLM into the aqueous phases or from the torus into the BLM. This technique, we feel, avoids the long waiting time required for a membrane to "absorb" the antibiotic from the aqueous phase, and avoids as well the problem of removal of the antibiotic from BLM by the torus (Benz *et al.*, 1973; Hladky, 1973).

The teflon cell is a simple modification of the type used by most workers (Fig. 4). A 10-mil teflon barrier with a 1.5 mm orifice is sandwiched between the two solution chambers.[6] The $\approx 3/8$ inch hole in the sandwiching face of each chamber is flared so that air bubbles cannot be trapped in the chamber around the orifice. The face of the rear

6 The primary virtue of the removable barrier is that it allows replacement of the orifice without rebuilding the entire cell system.

chamber has an O-ring, inset with a 5-mil protrusion, which exerts enough pressure on the barrier to prevent leaking. An optical window in the front chamber is large enough (1 inch diameter) to permit illumination of the membrane with an American Optical fiber optics light source and viewing with a Bausch and Lomb stereoscope. The black plug (fiberbase plastic – Franklin Fiber Lametex Corp.) in the rear chamber minimizes light reflection from the rear chamber and improves membrane visibility. Teflon tape or teflon gaskets are used to prevent leaking around the window and plug. The barrier orifice is drilled with a new drill while the barrier is sandwiched between two pieces of plexiglass or lucite. A silver wire coil electrode is permanently attached to each chamber.

Membranes are made using a Pasteur pipette as described by Szabo, Eisenman and Ciani (1969). Membrane size is determined using the microscope reticule. The tip of the pipette was fire polished prior to use—primarily to avoid damaging the orifice. Data reported here were obtained on "freshly thinned membranes" from $\frac{1}{2}$ to 3 min after going black. All experiments were carried out at 26 ± 1 °C.

The charge pulse generator was designed and built by the Instrumentation Division, Brookhaven National Laboratory, and included a high impedance voltage follower. A Biomation 802 transient recorder was interfaced to a Kennedy incremental tape transport (Model 1600). Magnetic tape reading and data print-out were obtained with a CDC 6600 computer. The Biomation 802 also operates as a data storage buffer and continuously displays the transient on a Tektronix oscilloscope. Thus, transients can be viewed before dumping the information onto the tape.

Results

Membrane Capacitance

Capacitance of the BLM was determined in two ways: (1) from the initial voltage change following the charge pulse and (2) from the rate of voltage decay across the membrane through an external resistor. This approach permits measurement of the capacitance over a large voltage range that is greatly extended by minimizing the time of exposure to high voltage.

The measurements were made on membranes with and without antibiotic. The values obtained in 3.0×10^{-3} moles/cm^3 LiCl and 1.0×10^{-3} mole/cm^2 CaCl were the same: 4.5×10^{-7} Farads/cm^2. A slightly higher value 4.8×10^{-7} Farads/cm^2, was obtained for 3.0×10^{-3} moles/cm^3 KCl. Sample results are shown in Fig. 5. The intercept voltage and the time constant for decay both give the value 4.5×10^{-7} Farads/cm^2. There is a slight convex curvature of the $\ln V - t$ decay which suggests that the capacitance of the membrane is slightly greater at the higher voltages (*see* White, 1974). This deviation from linearity was ignored and the value 4.5×10^{-7} Farads/cm^2 was assumed to be the voltage-independent capacitance of the membrane.

Steady-State Measurements of Actin-Mediated Ammonium Ion Transport: Nonactin, Monactin, Dinactin and Trinactin

The steady-state kinetic parameters for the transport of ammonium ion across a 5% GMO/*n*-decane BLM were deduced from charge pulse data.

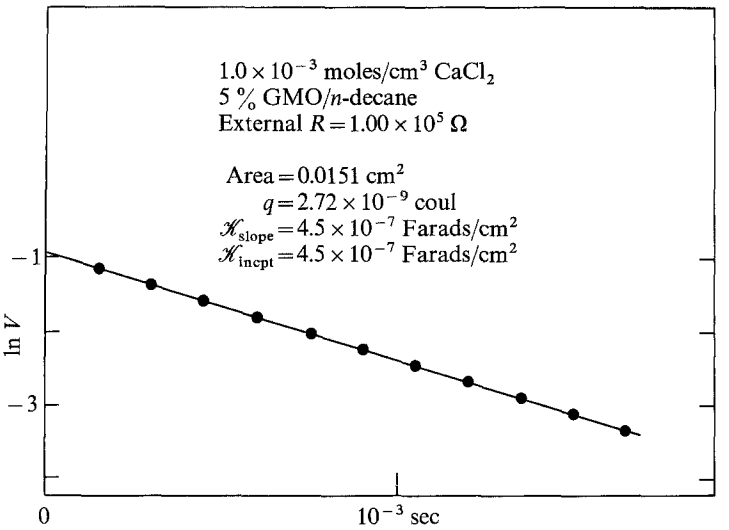

Fig. 5. Plot of ln *V vs.* time for the decay of charge on a GMO BLM through an external resistance (1.00×10^5 ohms)

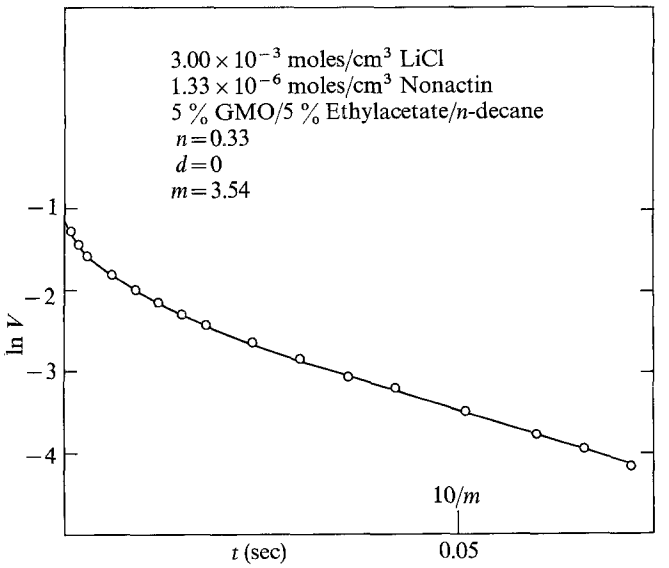

Fig. 6. Plot of ln *V vs.* time for decay of charge through a nonactin-mediated Li^+ transport mechanism. Open circles are experimental points and solid line is theoretical curve calculated from integration of Eq. (11) with: $n = 0.33$, $d = k_{is}^*/k_{-1} = 0$, and $10/m = 2.82 = F^2 \beta K_1 k_{is}^* c_i t/(RT\mathscr{K}_m)$, when $t = 0.05$ sec

To obtain the value of n, Eq. (11), charge pulse data were obtained for LiCl (3×10^{-3} moles/cm^3) and a mixture of NaCl (1×10^{-3} mole/cm^3) and LiCl (2×10^{-3} moles/cm^3) with nonactin (1.33×10^{-6} moles/cm^3 in 5% GMO/5% ethyl acetate/*n*-decane). The decay curves are virtually congruent

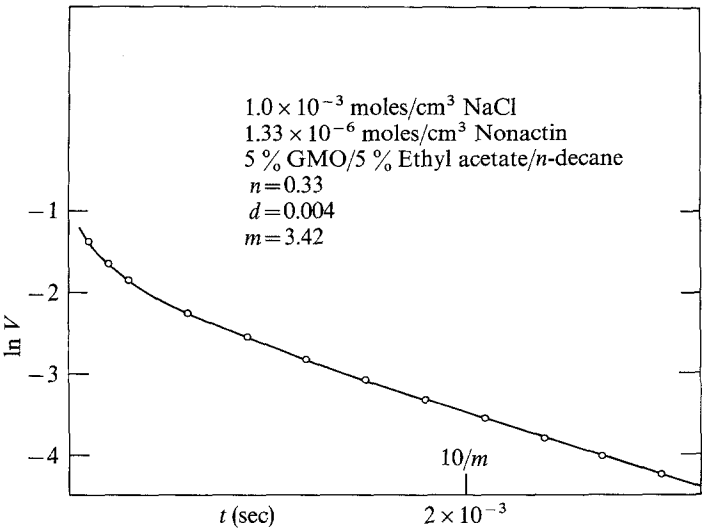

Fig. 7. Plot of ln V *vs.* time for decay of charge through a nonactin-mediated Na^+ transport mechanism. Open circles are experimental points and solid line is theoretical curve calculated from integration of Eq. (11) with: $n = 0.33$, $d = k_{is}^*/k_{-1} = 0.004$, and $10/m = 2.92 = F^2 \beta K_1 k_{is}^* c_i t/(RT\mathcal{K}_m)$, when $t = 2.0 \times 10^{-3}$ sec. Aqueous medium is 1.0×10^{-3} mole/cm^3 NaCl and 2.0×10^{-3} moles/cm^3 LiCl

(Figs. 6 and 7), consistent with the assumption that k_{-1} is large enough to make the denominator of Eq. (11) equal to unity. The value of n is 0.33. A slightly better fit to the NaCl data could be obtained assuming that $k_{is}^*/k_{-1} = 0.004$. The estimated contribution of background LiCl to the NaCl conductance is less than 2% and was ignored. Ethyl acetate (5%) was added to the membrane-forming mixture to improve the solubility of nonactin. Data for monactin (7.0×10^{-7} moles/cm^3 in 5% GMO/*n*-decane) in LiCl (3×10^{-3} moles/cm^3) are also consistent with $n = 0.33$. The remaining data that we report for the actins were obtained on membranes with no ethyl acetate. The background salt is $CaCl_2$ (1.0×10^{-3} mole/cm^3 $-\frac{1}{3}$ [NH_4Cl]). $CaCl_2$ has a nearly linear ln V *vs.* t decay curve corresponding to ohmic behavior. This behavior may be the manifestation of impurities in the $CaCl_2$. Nevertheless, the conductance of the BLM in $CaCl_2$ at high voltage ($\sim$0.4 volts) is at least a factor of 10 lower than for LiCl, making it an ideal background electrolyte.

Typical data for the decay curves with the actins are shown in Figs. 8 through 11. Low concentrations of the actins (6 to 7×10^{-8} moles/cm^3) are used to slow the voltage decay and ensure that the rate processes are at steady state. Only the shape parameter $k_{is}^*\left(1 + \frac{k_1 c_i}{2k_s}\right)\Big/k_{-1}$ and the scaling

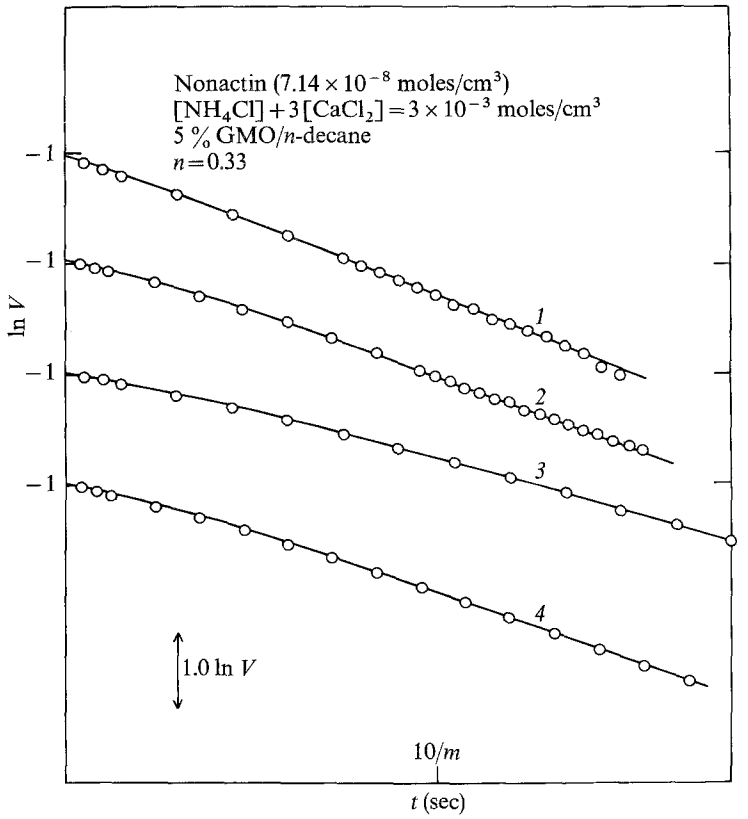

Fig. 8. Plot of ln V *vs.* time for decay of charge through a nonactin-mediated NH_4^+ transport mechanism. Open circles are experimental points and solid lines are theoretical curves calculated from integration of Eq. (11). For all curves: $n = 0.33$. For individual curves:

Curve	c_i (moles/cm^3)	k_{is}^*/k_{-1}	$F^2 \beta K_1 k_{is}^* c_i t/(RT\mathscr{K}_m)$	t (sec)
1	3.0×10^{-6}	0.25	4.69	2.0×10^{-2}
2	1.34×10^{-5}	0.28	4.50	5.0×10^{-3}
3	5.74×10^{-5}	0.28	3.50	1.0×10^{-3}
4	2.59×10^{-4}	0.28	4.27	5.0×10^{-4}

term $K_1 k_{is}^* \beta$ were adjusted in fitting the data. Two interesting points are immediately observable: (1) except for the lowest ammonium ion concentrations with trinactin the value of the shape parameter for a given actin remains constant with increasing ammonium ion concentration; and (2) the scaling term $K_1 k_{is}^* \beta$ diminishes with increasing concentration of ammonium ion. In the context of the model that is the basis of Eq. (11), one is forced

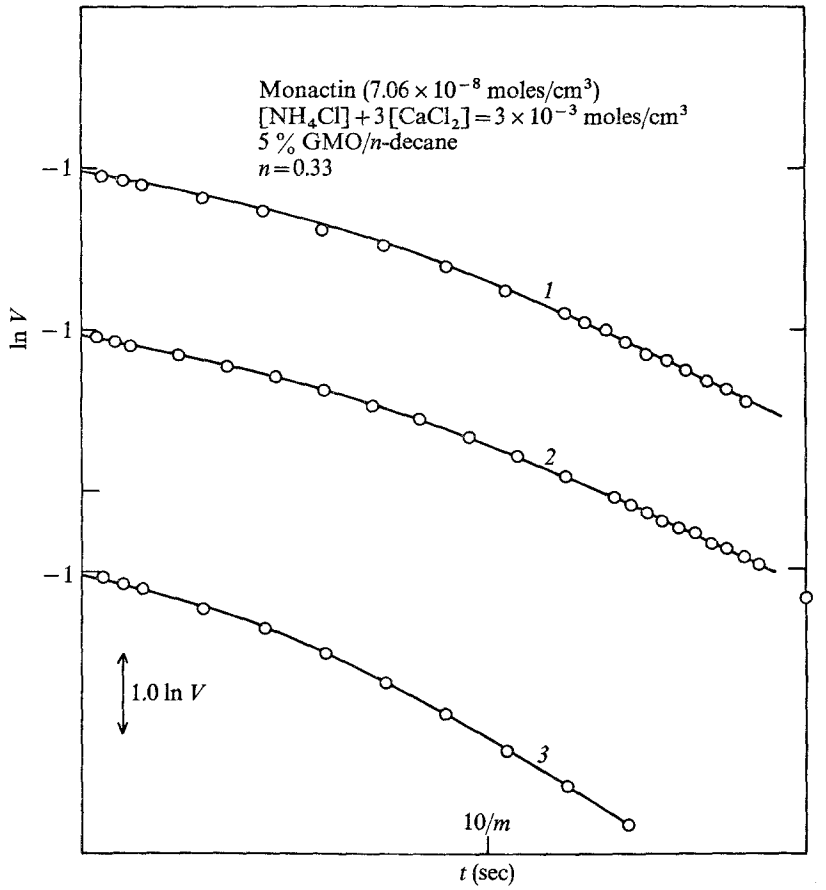

Fig. 9. Plot of ln V *vs.* time for decay of charge through a monactin-mediated NH_4^+ transport mechanism. Open circles are experimental points and solid lines are theoretical curves calculated from integration of Eq. (11). For all curves: $n = 0.33$ and $k_{is}^*/k_{-1} = 0.6$. For individual curves:

Curve	c_i (moles/cm^3)	$F^2 \beta K_1 k_{is}^* c_i t/(RT\mathscr{K}_m)$	t (sec)
1	3.75×10^{-6}	7.14	2.0×10^{-2}
2	1.42×10^{-5}	6.94	5.0×10^{-3}
3	2.60×10^{-4}	9.35	1.0×10^{-3}

to conclude that $k_1 c_i/k_s$ remains small compared to unity and that β is defined according to Eq. (6). The expansion of the inverse of the scaling-term is

$$\frac{1}{K_1 k_{is}^* \beta} = \frac{1}{K_1 k_{is}^* \Gamma_T} + \frac{c_i}{k_{is}^* \Gamma_T}. \tag{18}$$

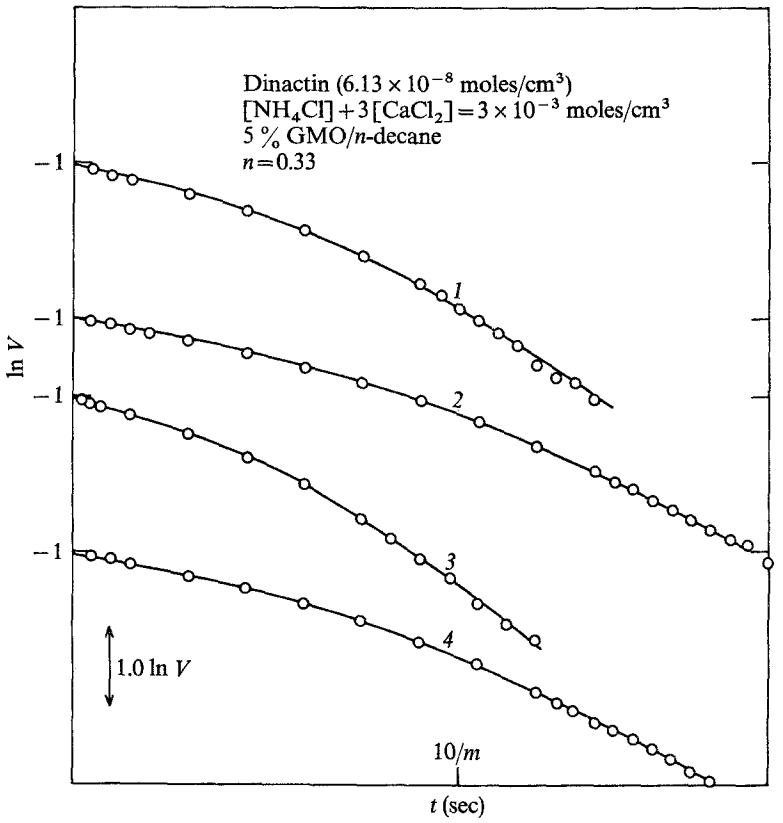

Fig. 10. Plot of ln V *vs.* time for decay of charge through a dinactin-mediated NH_4^+ transport mechanism. Open circles are experimental points and solid lines are theoretical curves calculated from integration of Eq. (11). For all curves: $n=0.33$ and $k_{is}^*/k_{-1}=0.8$. For individual curves:

Curve	c_i (moles/cm^3)	$F^2\beta K_1 k_{is}^* c_i t/(RT\mathscr{K}_m)$	t (sec)
1	4.5×10^{-6}	11.1	2.0×10^{-2}
2	2.48×10^{-4}	8.9	1.0×10^{-3}
3	1.15×10^{-4}	13.0	2.0×10^{-3}
4	3.68×10^{-4}	9.0	1.0×10^{-3}

Thus, a plot of the left-hand side of Eq. (18) *vs.* c_i should be linear, with the slope and intercept yielding the values of K_1 and $k_{is}^*\Gamma_T$. A sample plot for dinactin is shown in Fig. 12. It is typical of the results for all the actins except nonactin which exhibits a slight superlinear (concave upward) behavior. The steady-state data for the actins are compiled in Table 1*A*.

We are somewhat surprised that the total carrier concentration in the BLM, Γ_T, remains constant with increasing $c_i(NH_4^+)$. We had expected that

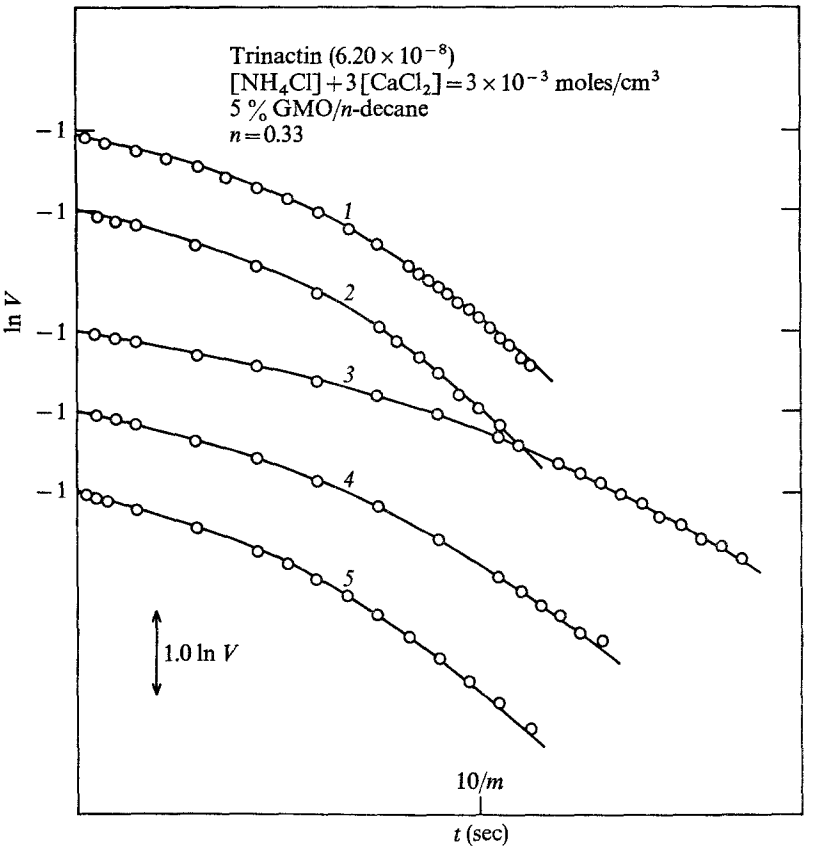

Fig. 11. Plot of ln V *vs.* time for decay of charge through a trinactin-mediated NH_4^+ transport mechanism. Open circles are experimental points and solid lines are theoretical curves calculated from Eq. (11). For all curves: $n=0.33$. For individual curves:

Curve	c_i (moles/cm^3)	k_{is}^*/k_{-1}	$F^2\beta K_1 k_{is}^* c_i t/(RT\mathscr{K}_m)$	t (sec)
1	5.9×10^{-6}	1.4	20.4	2.0×10^{-2}
2	1.34×10^{-5}	1.4	22.0	1.0×10^{-2}
3	1.28×10^{-4}	1.0	10.9	2.0×10^{-3}
4	2.19×10^{-4}	1.0	14.1	1.0×10^{-3}
5	4.88×10^{-4}	1.0	16.4	1.0×10^{-3}

a rapid equilibrium would be established at the boundary between a blackened and as yet unblackened region of the membrane and that Γ_s would be effectively buffered. The data clearly contradict this expectation – for the actins. As we will demonstrate valinomycin *does* behave according to expectation.

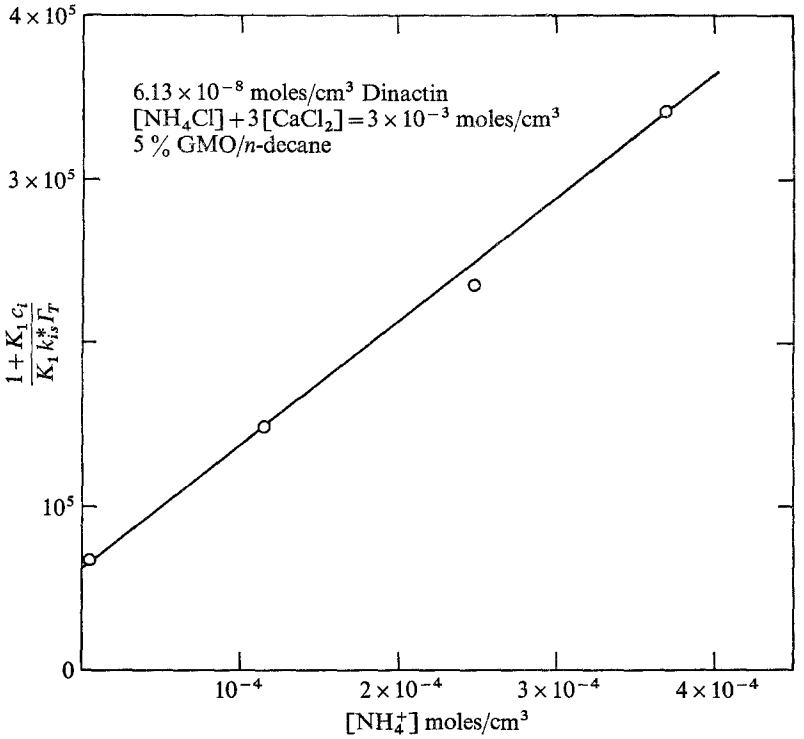

Fig. 12. Plot of $1/(K_1 k_{is}^* \beta)$ *vs.* c_i for dinactin-mediated NH_4^+ transport

Measurement of Γ_T for the Actins

The fact that Γ_T is maintained constant, in addition to yielding information about K_1 and $k_{is}^* \Gamma_T$, allows us to measure Γ_{is} easily using the principles outlined in the Theory section. Five different concentrations of trinactin in 5% GMO/*n*-decane were prepared: 0, 1.55×10^{-7}, 3.1×10^{-7}, 4.65×10^{-7}, and 6.1×10^{-7} moles/cm^3. The electrolyte for this experiment was a mixture of NH_4Cl (5×10^{-4} moles/cm^3) and $CaCl_2$ (8.3×10^{-4} moles/cm^3). The capacitance of a membrane with no trinactin was measured using the charge pulse technique and noting the voltage decay through a 2000-ohm resistor across the electrodes. This permitted us to charge the membrane up to about 0.4 volts. Both the intercept and slope of the $\ln V$ *vs.* t plot were consistent with a membrane capacitance of 4.5×10^{-7} Farads/cm^2. The resistor was removed and the charge pulse experiments were carried out on the membranes containing trinactin. About 5 to 10 μsec after the charge pulse there begins a well defined linear decay of the voltage *vs.* time. The extrapolated zero-time intercept of this linear region gives a voltage measurably lower than that predicted on the basis of the magnitude of the charge pulse, membrane

Table 1. *A*. Steady-state parameters for actin-mediated transport of NH_4^+

Actin	c_s	$K_1 k_{is}^* \Gamma_T$	$\frac{k_{is}^*}{k_{-1}}$	K_1	$k_{is}^* \Gamma_T$	$k_1 \Gamma_T$
Nonactin	7.1×10^{-8}	9×10^{-6}	0.28	4.8×10^{3}	1.9×10^{-9}	3.2×10^{-5}
Monactin	7.1×10^{-8}	1.3×10^{-5}	0.6	7.5×10^{3}	1.7×10^{-9}	2.2×10^{-5}
Dinactin	6.1×10^{-8}	1.6×10^{-5}	0.8	1.2×10^{4}	1.3×10^{-9}	2.1×10^{-5}
Trinactin	6.2×10^{-8}	1.2×10^{-5}	1.0	1.0×10^{4}	1.2×10^{-9}	1.2×10^{-5}

B. Evaluation of Γ_T for actins $[NH_4^+]=5.0\times10^{-4}$ moles/cm^3

Actin	c_s	Γ_{is}	Γ_T	Γ_T/c_s	exptl. dV/dt	calc.[a] dV/dt
Nonactin	7.1×10^{-7}	1.2×10^{-12}	1.7×10^{-12}	2.5×10^{-6}	1.0×10^{4}[b]	1.0×10^{4}[b]
Monactin	7.1×10^{-7}	9.9×10^{-13}	1.3×10^{-12}	1.8×10^{-6}	4.2×10^{3}	5.0×10^{3}
Dinactin	6.1×10^{-7}	8.6×10^{-13}	9.9×10^{-13}	1.6×10^{-6}	3.0×10^{3}	3.2×10^{3}
Trinactin	6.2×10^{-7}	7.8×10^{-13}	9.5×10^{-13}	1.5×10^{-6}	1.8×10^{3}	2.1×10^{3}

[a] Calculated from data in Table 1 *A*. (Note c_s's and $\therefore$ Γ_T's are a factor of 10 different.)
[b] Straight line portion for nonactin only is poorly defined; calculated value was used to help define line.

C. Estimated rate parameters for actins (from data in Tables *A* and *B*)

Actin	k_{is}^*	k_1	k_{-1}	k_s[a]
Nonactin	1.1×10^{4}	1.8×10^{8}	4.3×10^{4}	$> 3\times10^{5}$
Monactin	1.3×10^{4}	1.7×10^{8}	2.2×10^{4}	$> 2\times10^{5}$
Dinactin	1.3×10^{4}	2.1×10^{8}	1.6×10^{4}	$> 3\times10^{5}$
Trinactin	1.3×10^{4}	1.2×10^{8}	1.3×10^{4}	$>1.5\times10^{5}$

[a] Assume that $k_1 c/2k_s<0.2$ and $\therefore$ $k_s>2.5\times k_1 c_i$, max.

area and membrane capacitance. We calculate Γ_{is} assuming that it alone is responsible for the intercept discrepancy. This is consistent with the previously deduced small value of $k_1 c_i/k_s$ (*see* Fig. 3). Then

$$\Gamma_T=\Gamma_{is}\frac{(1+K_1 c_i)}{K_1 c_i}. \tag{19}$$

A plot of Γ_{is} value *vs.* the bulk concentration, c_s, of trinactin is satisfyingly linear (Fig. 13). Corresponding values for the other actins were measured, but only at a single concentration. The results are presented in Table 1 *B*. The calculated values for the linear voltage decay are calculated from the

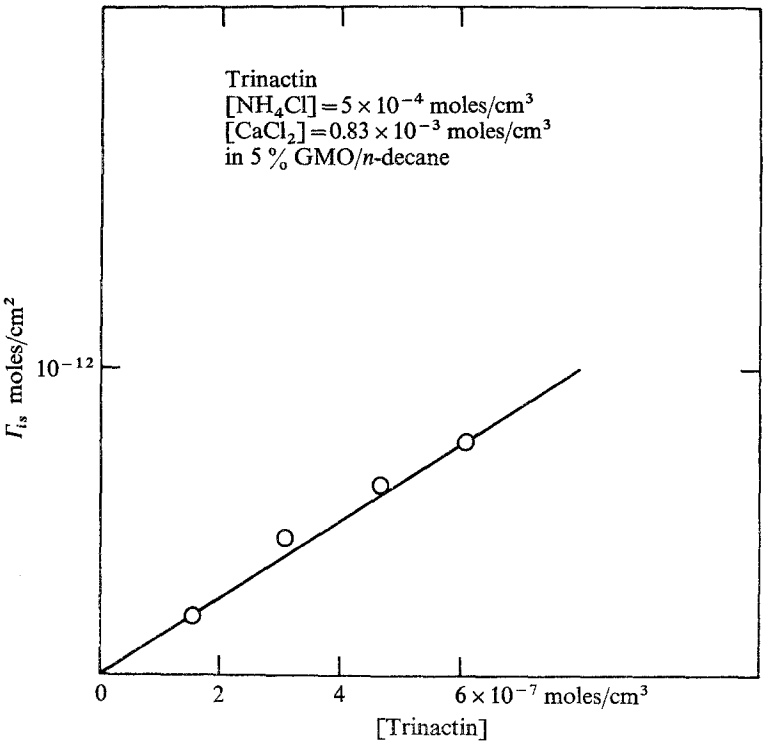

Fig. 13. Plot of Γ_{is} *vs.* c_s for trinactin-mediated NH_4^+ transport

high voltage limiting form of Eq. (11):

$$\frac{dV}{dt} = \frac{J_{is}F}{\mathscr{K}_m} = \frac{F}{\mathscr{K}_m} \frac{k_1 \Gamma_T c_i}{(1+K_1 c_i)}. \tag{20}$$

The calculated value of dV/dt in the linear voltage decay region is based on the steady-state data in Table 1 *A*. The agreement is quite good. In the case of nonactin, however, the linear decay is so poorly defined that we used the calculated value to locate the region of linear decay and the appropriate intercept. The problem is due in part to the relatively high concentration of nonactin in the BLM and the fact that once the carrier complex had moved across the membrane the voltage had dropped too low for Eq. (20) to be valid over a large enough voltage range. A lower value of c_s for the nonactin would have improved the analysis. Analysis of the data for $c_s = 7.1 \times 10^{-8}$ gave nearly the same result.

The value of K_1 permits us to estimate the change in the value of Γ_{is} with c_i. Assuming a constant value of Γ_T, the value of Γ_{is} for any of the actins

increases only slightly at higher concentrations of ammonium ion. The prediction was tested and verified for nonactin and ammonium ion ($K_1 = 4.8 \times 10^3$ moles/cm^3 and 4×10^{-4} moles/cm$^3 < c_i < 1.25 \times 10^{-3}$ moles/cm^3). This is direct evidence that Γ_T does remain constant.

The measured values of the ratio Γ_T/c_s (Table 1*B*) agree with Hladky's (1973) estimate of 3×10^{-6} moles/cm^3 for nonactin in GMO.

On the basis of the data presented in Tables 1*A* and 1*B* we can calculate values for rate constants k_{is}^*, k_1, and k_{-1} (Table 1*C*).[7] Only a lower limit for k_s can be estimated. We assume that a 20% variation in the parameter $1 + k_1 c_i/(2k_s)$ would measurably affect the shape of the voltage decay curve[8] and we see no such changes. Thus we can write:

$$k_s > 2.5\, k_1\, c_{i,\max} \tag{21}$$

where $c_{i,\max}$ is the highest value of c_i used.

Several interesting facts emerge from the data in Table 1*C*. First is the constancy of the rate parameter k_{is}^* for all the actins. This suggests that the membrane energy barrier for the four different ammonium-actin complexes is essentially the same.[9] Second is the observation that k_s is much greater than k_{is}^*. Laprade, Ciani, Eisenman and Szabo (1974) made a similar observation in studies of actin-mediated transport in glycerol dioleate membranes (GDO) (*see* Table 3) and rationalize it by pointing out that the carrier complex must overcome the dielectric energy barrier as discussed by Neumcke and Läuger (1970). Laprade *et al.* (1974) also noted that the values of the instantaneous current (for high concentrations of NH_4^+ with trinactin in GDO) predicted from steady-state data were much higher than the values directly measured using voltage-clamp techniques. If k_s is as large ($> 3 \times 10^5$ sec^{-1}) in GDO as in GMO, then the instantaneous current should be greater than the steady-state current by a constant factor independent of the ammonium-ion concentration. This may be deduced mathematically as follows for the zero voltage condition ($u \to 0$):

$$\frac{J_{is}(V=0,\, t=0)}{u} = \tfrac{1}{2} k_{is}^* K_1\, c_i \beta \tag{22}$$

7 The reader is reminded that rate constant k_1 cm^3 moles^{-1} sec^{-1} will be 1000 times larger than the equivalent constant expressed in units liter moles^{-1} sec^{-1}.

8 This presumes $k_{is}^*(1 + k_1 c_i/(2k_s))/k_{-1} < 1.5$. Changes in larger values of this parameter have a diminished effect on shape changes in the voltage decay curve.

9 This supports the conclusion of Szabo, Eisenman and Ciani (1969) that the overall size and shape of the actin antibiotics are independent of the degree of methylation.

and from Eq. (11) for $k_s \to \infty$ and $u \to 0$

$$\frac{J_{is}(V=0, t=\infty)}{u} = \frac{\frac{1}{2} k_{is}^* K_1 c_i \beta}{1 + \frac{k_{is}^*}{k_{-1}}} \tag{23}$$

and $\therefore$

$$\frac{G(V=0, t=0)}{G(V=0, t=\infty)} = \frac{J_{is}(V=0, t=0)}{J_{is}(V=0, t=\infty)} = 1 + \frac{k_{is}^*}{k_{-1}}. \tag{24}$$

This ratio ought to be valid regardless of how the carrier is introduced into the membrane. For trinactin-mediated transport of ammonium ion in GMO this ratio is about 2 (*see* Table 1*A*) and this concurs with the experimental observations of Laprade *et al.* (1974) albeit for GDO. We agree with them that this discrepancy may well reflect an inadequacy in the model. With the exception of the value of k_s, however, their data and ours agree well (*see* Table 3).

The calculated values of the steady-state conductance ratio $\frac{G(V, t=\infty)}{G(V=0, t=\infty)}$ as a function of voltage for the four actins are shown in Fig. 14. These are calculated from the following equation:

$$\frac{G(V, t=\infty)}{G(V=0, t=\infty)} = \frac{(J_{is}/u)_V}{(J_{is}/u)_{V=0}} \tag{25}$$

where J_{is} is calculated from Eq. (11) using the appropriate data in Table 1*A*. The data of Laprade *et al.* (1974) for trinactin-NH_4^+ transport is plotted for comparison (solid dots) using their version of a modified single barrier model. Our data predict virtually no effect of increasing c_i. Their lower values of k_s, on the other hand, predict a change in the shape of the curves in Fig. 14 with increasing c_i.

Steady-State Data for Valinomycin

To establish the value of n in Eq. (11) the charge-pulse experiment was carried out on a 5% GMO/*n*-decane membrane containing 3.68×10^{-6} moles/cm^3 valinomycin with $3 = 10^{-3}$ moles/cm^3 NaCl in both chambers. A good fit was obtained for $n = 0.26$ (Fig. 15). We felt that the conductance of the membrane in 3×10^{-3} moles/cm^3 LiCl was too close to background (i.e. the conductance level of a membrane with no valinomycin) for a valid determination of n. Thus, unlike the case for the actins, where we obtained identical values of n for NaCl and LiCl, we have no real assurance that we are observing behavior in the equilibrium domain.

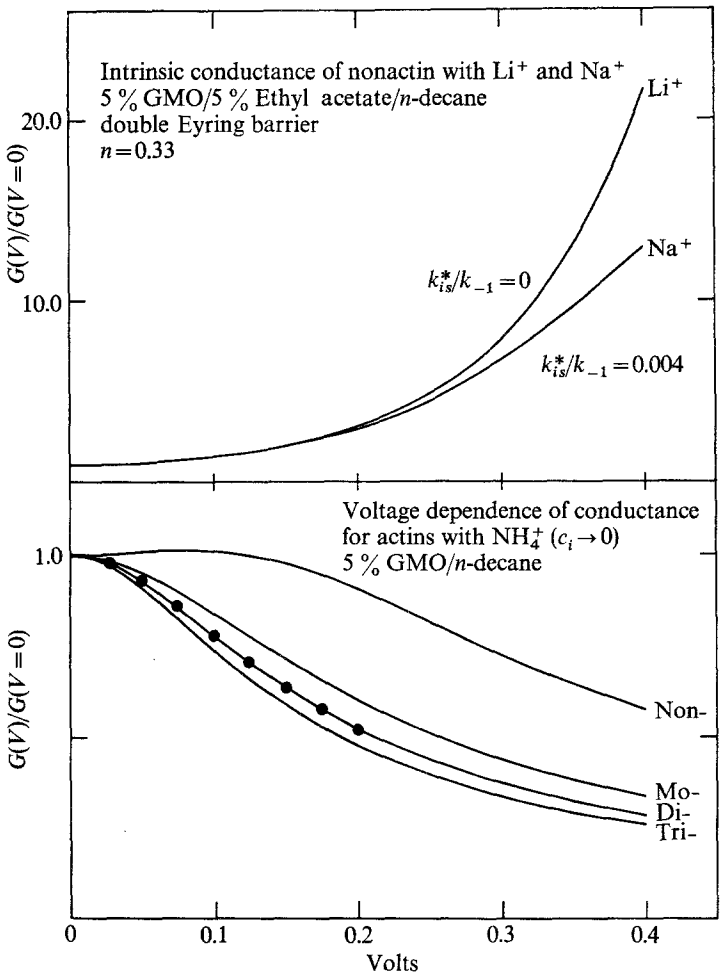

Fig. 14. Steady-state conductance ratios $(G(V, t=\infty)/G(V=0, t=\infty))$ for the actins. Curves are calculated from Eq. (25) and data in Table 1*A*. Points are calculated from data of Laprade, Ciani, Eisenman and Szabo (1974) using $k_{is}^*/k_{-1}=1.8$ for trinactin-NH_4^+ transport on GDO membranes and the equation:

$$\frac{G(V, t=\infty)}{G(V=0, t=\infty)} = \frac{(1+k_{is}^*/k_{-1})\sinh(bu)}{bu(1+k_{is}^*\cosh(bu)/k_{-1})}$$

where $b=0.36$. This equation differs slightly from theirs because of the redefinition of k_{is}^*/k_{-1} (*see* footnote 4)

In experiments with CsCl and KCl (ionic strength maintained at 3×10^{-3} moles/cm^3 with LiCl) we used a lower concentration of valinomycin (8.85×10^{-8} moles/cm^3) to ensure that the voltage decay time constants are long enough for the rate processes to be at steady state. The

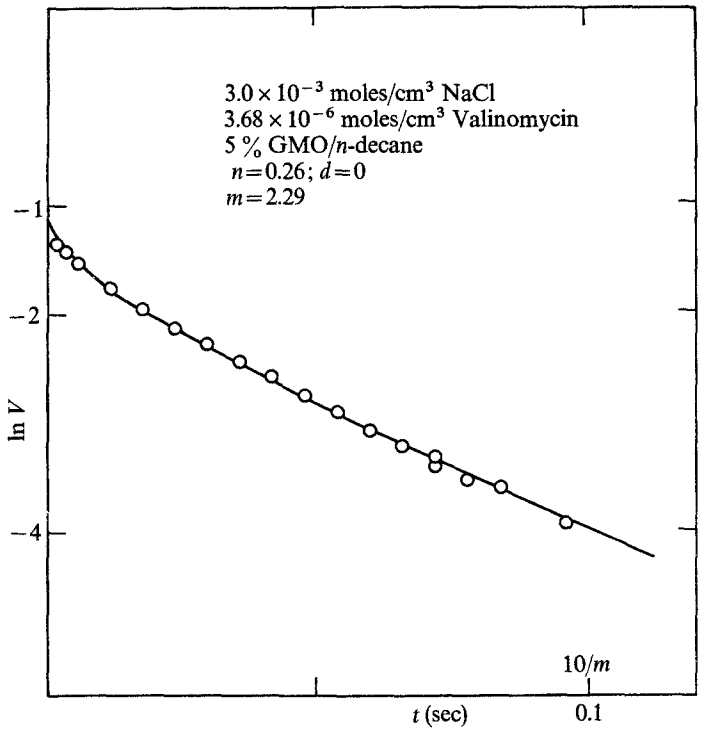

Fig. 15. Plot of $\ln V$ *vs.* time for decay of charge through a valinomycin-mediated Na^+ transport mechanism. Open circles are experimental points and solid line is theoretical curve calculated from integration of Eq. (11) with: $n=0.26$, $d=k_{is}^*/k_{-1}=0$, and $10/m=4.37=F^2\beta K_1 k_{is}^* c_i t/(RT\mathscr{K}_m)$, when $t=0.1$ sec

change in curve shape with increasing KCl or CsCl concentration (Figs. 16 and 17) is indicative of the increasing value of the ratio $k_1 c_i/(2k_s)$ in Eq. (11). A plot of the parameter $\frac{k_{is}^*}{k_{-1}}\left(1+\frac{k_1 c_i}{2k_s}\right)$ *vs.* c_i allows us to estimate both k_{is}^*/k_{-1} and k_1/k_s. The value of $K_1 k_{is}^* \beta$ remains constant, consistent with $\beta=\Gamma_s$ (*see* Eqs. (5) and (6) and accompanying text). The steady-state data for CsCl and KCl are collected in Table 2.

It is particularly interesting to us that it is Γ_s which appears to be buffered during the membrane formation (unlike the case for the actins where it is Γ_T that seems to be maintained constant). In the case of the Cs^+ transport we are confident this is the case. The potassium data presents a problem in that once

$$\frac{k_{is}^*}{k_{-1}}\left(1+\frac{k_1 c_i}{2k_s}\right)>2 \tag{26}$$

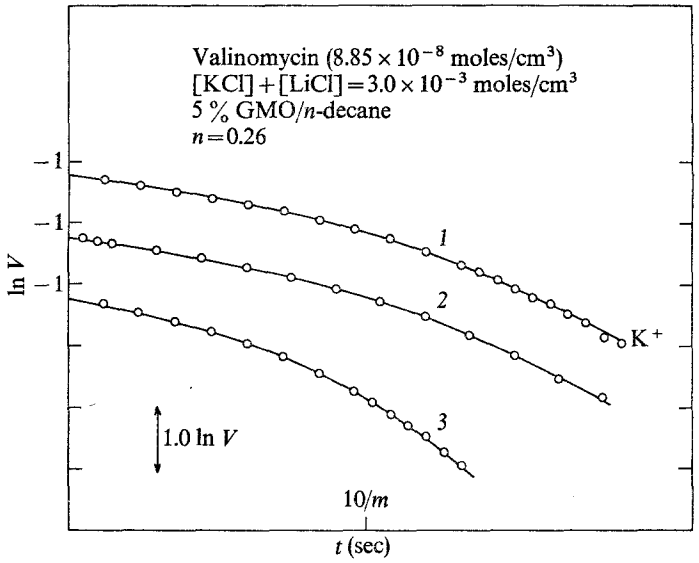

Fig. 16. Plot of $\ln V$ *vs.* time for decay of charge through a valinomycin-mediated K^+ transport mechanism. Open circles are experimental points and solid lines are theoretical curves calculated from Eq. (11). For all curves $n=0.26$. For individual curves:

Curve	c_i (moles/cm^3)	$\frac{k_{is}^*}{k_{-1}}\left(1+\frac{k_1 c_i}{2k_s}\right)$	$F^2\beta K_1 k_{is}^* c_i t/(RT\mathcal{K}_m)$	t (sec)
1	7.5×10^{-6}	1.6	12.5	5.0×10^{-2}
2	4.7×10^{-5}	2.10	15.6	1.0×10^{-2}
3	1.85×10^{-4}	3.15	30.8	5.0×10^{-3}

Table 2. Steady-state parameters for valinomycin-mediated transport
$c_s = 8.85 \times 10^{-8}$ moles/cm^3

Ion	$K_1 k_{is}^* \Gamma_s$ cm sec	$k_{is}^*/k-1$	k_1/k_s	$k_s\Gamma_s$
Cs^+	1.8×10^{-6}	0.4	1.6×10^4	2.4×10^{-10}
K^+	4.0×10^{-6}	1.6	1.06×10^4	2.8×10^{-10}

the effect of the shape of the voltage decay is negligible and one effectively only changes the scaling. Thus, in fitting the potassium data, we assumed that the scaling parameter, $K_1 k_{is}^* \Gamma_s$ remains constant. The assumption is supported by the comparative values of term $k_s\Gamma_s$ for Cs^+ and K^+ transport. It is clear, of course, that these values must be identical.

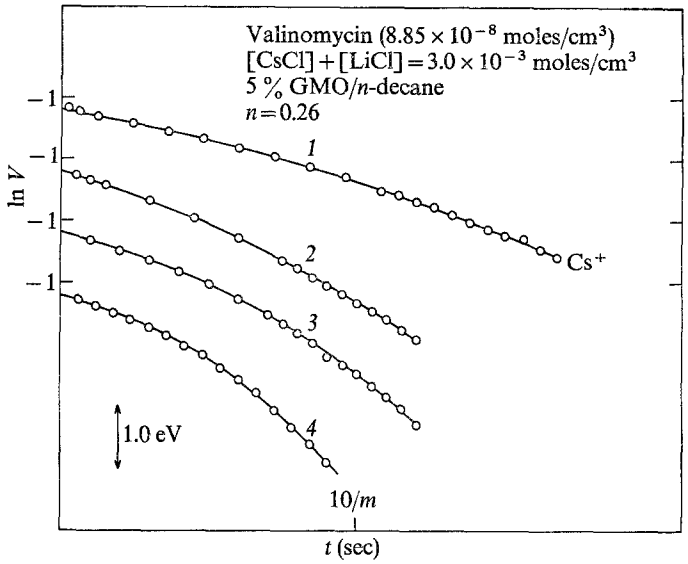

Fig. 17. Plot of ln V *vs.* time for decay of charge through a valinomycin-mediated Cs^+ transport mechanism. Open circles are experimental points and solid lines are theoretical curves calculated from Eq. (11). For all curves $n = 0.26$. For individual curves:

Curve	c_i (moles/cm^3)	$\frac{k_{is}^*}{k_{-1}}\left(1+\frac{k_1 c_i}{2k_s}\right)$	$F^2 \beta K_1 k_{is}^* c_i t/(RT\mathcal{K}_m)$	t (sec)
1	7.5×10^{-6}	0.5	5.46	5.0×10^{-2}
2	5.2×10^{-5}	0.5	8.5	1.0×10^{-2}
3	2.09×10^{-4}	1.0	14.5	5.0×10^{-3}
4	3.33×10^{-4}	1.5	24.8	5.0×10^{-3}

Measurement of Γ_{is} and Γ_T for Valinomycin

Measurement of the intercept discrepancy is not as straightforward for valinomycin as for the actins. This is due, in part, to the larger values of $k_1 c_i/k_s$ that obtain. It appears that we can discern two intercepts corresponding to V_2 and V_3 as discussed in the Theory section. The analysis is further complicated, however, because the voltage diminishes below the value necessary to maintain the conditions $k'_{is} = \infty$. We cannot simply increase q^0 since the initial voltage would be high enough to break the membrane. Thus, proper analysis of this data will require the complete time-dependent analysis of the sort indicated in Fig. 3, perhaps with consideration of the additional variables k_{is}^*, u, and n.

The buffering of Γ_s rather than Γ_T precludes the simple experiments where c_i is increased and K_1 deduced as was done with the actins. Experi-

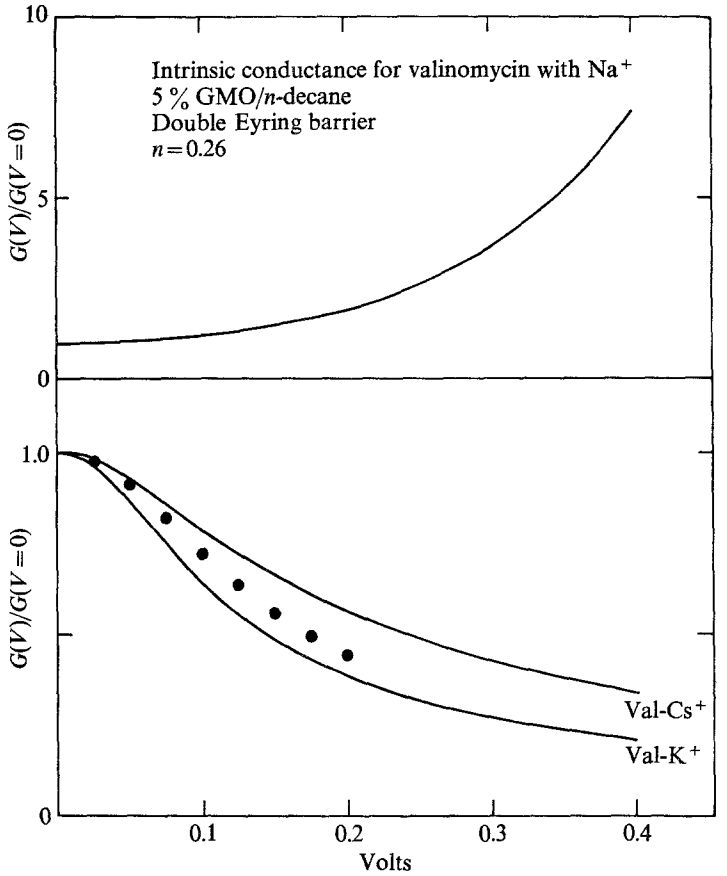

Fig. 18. Steady-state conductance ratios ($G(V, t=\infty)/G(V=0, t=\infty)$) for valinomycin-mediated transport of Na^+, Cs^+, and K^+ as $c_i \to 0$. Curves are calculated from Eq. (25) and data in Table 2. Points are calculated from data of Laprade, Ciani, Eisenman and Szabo (1974) using their value $k_{is}^*/k_{-1}=1.3$ for valinomycin-K^+ transport on GDO membranes. The equation given in the caption for Fig. 14 was used with $b=0.5$

mental modification can, in principal, circumvent some of these difficulties (*see* final section).

On the basis of our present data we can tentatively estimate that Γ_s/c_s for valinomycin is about 2×10^{-8} cm, approximately two orders of magnitude smaller than our calculated values of Γ_T/c_s for the actins (note that as $c_i \to 0$, $\Gamma_T \to \Gamma_s$). If this estimate is correct, the difference in the nature of the buffering for valinomycin and the actins may be simply explained by a difference in "buffer capacity", i.e., the concentration of carrier in the blackened membrane relative to that in the unblackened membrane (which we assume to be identical to the bulk lipid-hydrocarbon-carrier mixture)

Table 3. Comparison of our data with that of Laprade, Ciani, Eisenman and Szabo (1974)

Constant	Trinactin-NH_4^+		Valinomycin-K^+	
	Laprade *et al.* (GDO)	This work (GMO)	Laprade *et al.* (GDO)	This work [a] (GMO)
k_{is}^{*} [b]	1.7×10^4	1.3×10^4	9.8×10^4	7.5×10^5
k_s	4.4×10^4	$>1.5\times10^5$	9.0×10^4	1.6×10^5
k_1	6.6×10^7	1.2×10^8	7.4×10^7	1.7×10^9
k_{-1}	9.2×10^3	1.2×10^4	7.4×10^4	4.7×10^5
K_1	7.2×10^3	1.0×10^4	1.0×10^3	3×10^3
k_1/k_s	1.5×10^3	$<8\times10^2$	8.2×10^2	1.1×10^4
k_{is}^{*}/k_{-1} [b]	1.80	1.0	1.3	1.6

[a] These constants derived on the basis of tentative estimates of $\Gamma_s/c_s\approx2\times10^{-8}$ and $K_1\approx3\times10^3$ deduced using the intercept discrepancy method.
[b] The value obtained by Laprade *et al.* (1974) must be doubled (*see* footnote 4).

is much smaller for valinomycin than for the actins. Thus, carrier transport across the boundary between the black and unblackened membrane areas may be limiting in one case (the actins) and not in the other (valinomycin).

Plots of $G(V, t=\infty)/G(V=0, t=\infty)$ as a function of voltage for valinomycin with Cs^+ and K^+ are shown in Fig. 18.

The comparison of our valinomycin-K^+ data with that of Laprade *et al.* (1974) (Table 3) does not exhibit nearly as good agreement as the trinactin-NH_4^+ data. Only the values of k_s and K_1 are in reasonable agreement. Nevertheless the voltage dependency of $G(V, t=\infty)/G(V=0, t=\infty)$ in the limit as $c_i\to0$ is quite similar for their system and ours (Fig. 18). Because of the tentativeness of our numbers we are reluctant to overanalyze the discrepancies between the two sets of data.

Prognosis for the Charge Pulse Technique and Some Experimental Modifications

The data we have presented here demonstrate many of the stated virtues of the charge pulse technique. Because of the extremely fast kinetics involved in the particular systems that we studied, our instrumentation was not fast enough for precise analysis of the time-dependent portion of the voltage decay curve. A faster pulser (*see* footnotes 1 and 2) and faster data acquisition will facilitate that aspect of study.

A simple modification of the technique described in the present work is the use of multiple charge pulses. This will allow one to boost the decay-

ing voltage back to a level where the condition $k'_{is} = \infty$ obtains and thereby minimize theoretical complexities. Furthermore, by using multiple charge pulses rather than a single large charge pulse, one can stay below the membrane breakdown voltage. For carriers such as valinomycin where Γ_s is buffered and Γ_{is} builds up in proportion to the K_1 and c_i of the complexed ion it may be advantageous to allow the membrane to form under conditions where $c_i = 0$, and then increase c_i to the desired value *after* the BLM has formed. The difficulty is simultaneously to homogenize the aqueous phases and minimize agitation of the membrane (and thereby minimize equilibration of the BLM with the torus).

A major task ahead of us is the development of the time-dependent theory describing the manifestations of various transport mechanisms in the charge pulse experiment. We anticipate that most of these calculations will be numerical requiring graphical presentation similar to Fig. 3.

We are particularly grateful to a number of investigators whose help has been invaluable to us in initiating and carrying out these studies: George Eisenman, Sally Krasne, Raynald Laprade, Stuart McLaughlin, and Gabor Szabo. We would also like to thank Timothy Brumleve, Robert Doering and Marc Fajer whose efforts in the early stages of this work were most useful. Miss Barbara Stearns of the Squibb Institute for Medical Research and Dr. Hans Bickel of the CIBA Pharmaceutical Company are thanked for their generous gifts of the actin homologues.

This work was performed under the auspices of the United States Atomic Energy Commission.

Note Added in Proof: Dr. S. B. Hladky has kindly informed us of the results of his recent studies of nonactin- and trinactin-mediated transport of alkali ions in GMO bilayers (*Biochim. Biophys. Acta, in press*). His values for the rate constants describing ammonium-ion transport (deduced from steady-state and voltage-clamp data) and ours agree reasonably well with the exception of the values of k_s for which he obtains nearly the same values as Laprade *et al.* (1974).

References

Benz, R., Stark, G., Janko, K., Läuger, P. 1973. Valinomycin-mediated ion transport through neutral lipid membranes: Influence of hydrocarbon chain length and temperature. *J. Membrane Biol.* **14**:339

Ciani, S. M., Eisenman, G., Laprade, R., Szabo, G. 1973. Theoretical analysis of carrier-mediated electrical properties of bilayer membranes. *In:* Membranes, A Series of Advances. G. Eisenman, editor. Vol. 2, p. 61. Marcel Dekker, New York

Daum, P. H., Enke, C. G. 1969. Electrochemical kinetics of the ferri-ferrocyanide couple on platinum. *Analyt. Chem.* **41**:653

Delahay, P. 1962. Coulostatic method for kinetic study of fast electrode processes. I. Theory. *J. Phys. Chem.* **66**:2204

Hall, J. E., Mead, C. A., Szabo, G. 1973. A barrier model for current flow in lipid bilayer membranes. *J. Membrane Biol.* **11**:75

Hladky, S. B. 1972. The steady-state theory of the carrier transport of ions. *J. Membrane Biol.* **10**:67

Hladky, S. B. 1973. The effect of stirring on the flux of carriers into black lipid membranes. *Biochim. Biophys. Acta* **307**:261

Hodgkin, A. L., Huxley, A. F., Katz, B. 1952. Measurement of current voltage relations in the membrane of the giant squid axon of *Loligo*. *J. Physiol.* **116**:424

Hsu, M., Chan, S. I. 1973. Nuclear magnetic resonance studies of the interaction of valinomycin with unsonicated lecithin bilayers. *Biochemistry* **12**:3872

Kudirka, J. M., Daum, P. H., Enke, C. G. 1972. Comparison of coulostatic data analysis techniques. *Analyt. Chem.* **44**:309

Kudirka, J. M., Enke, C. G. 1972. Use of higher overvoltages in coulostatic kinetic measurements. *Analyt. Chem.* **44**:614

Laprade, R., Ciani, S. M., Eisenman, G., Szabo, G. 1974. The kinetics of carrier-mediated ion permeation in lipid bilayers and its theoretical interpretation. *In:* Membranes, A Series of Advances. G. Eisenman, editor. Vol. 3. Marcel Dekker, New York

Läuger, P., Stark, G. 1970. Kinetics of carrier-mediated ion transport across lipid bilayer membranes. *Biochim. Biophys. Acta* **211**:458

McConnell, H. M. 1974. Molecular Motion in Membranes. Presented at the 167th Amer. Chem. Soc. Meet., Los Angeles, California, March 31—April 5

Marcus, R. A. 1963. On the theory of oxidation-reduction reactions involving electron transfer. V. Comparison and properties of electrochemical and chemical rate constants. *J. Phys. Chem.* **67**:853

Mohilner, D. M. 1966. The electrochemical double layer. Part I. Elements of double-layer theory. *In:* Electroanalytical Chemistry. A. J. Bard, editor. Vol. 1, p. 241. Marcel Dekker, New York

Neumke, B., Läuger, P. 1970. Nonlinear electrical effects in lipid bilayer membranes. II. Integration of the generalized Nernst-Planck equations. *Biophys. J.* **9**:1160

Reinmuth, W. H. 1962. Theory of coulostatic impulse relaxation. *Analyt. Chem.* **34**:1272

Seelig, J., Niederberger, W. 1974. Two pictures of a lipid bilayer. A comparison between deuterium-label and spin-label experiments. *Biochemistry* **13**:1585

Stark, G., Benz, R. 1971. The transport of potassium through lipid bilayer membranes by the neutral carriers valinomycin and monactin. Experimental studies to a previously proposed model. *J. Membrane Biol.* **5**:133

Stark, G., Ketterer, B., Benz, R., Läuger, P. 1971. The rate constants of valinomycin-mediated ion transport through thin lipid membranes. *Biophys. J.* **11**:981

Szabo, G., Eisenman, G., Ciani, S. 1969. The effects of the macrotetralide actin antibiotics on the electrical properties of phospholipid bilayer membranes. *J. Membrane Biol.* **1**:346

Weir, W. D., Enke, C. G. 1967. The current-impulse relaxation techniques and the kinetics of rapid electrochemical reaction. I. General considerations. II. The electrochemical reduction of mercury (I). *J. Phys. Chem.* **71**:275, 280

White, S. M. 1974. Comments on "electrical breakdown of bimolecular lipid membranes as an electrochemical instability". *Biophys. J.* **14**:155